RSC Advances

ROYAL SOCIETY OF CHEMISTRY

www.rsc.org/advances

Cotton-based porous activated carbon with large specific surface area as electrode material for high-performance supercapacitor

Guofu Ma[a*], Dongyang Guo[a], Kanjun Sun[b], Hui Peng[a],

Qian Yang[a], Xiaozhong Zhou[a], Xiaolong Zhao[a], Ziqiang Lei[a]*

[a]*Key Laboratory of Eco-Environment-Related Polymer Materials of Ministry of Education, Key Laboratory of Polymer Materials of Gansu Province, College of Chemistry and Chemical Engineering, Northwest Normal University, Lanzhou 730070, China.*

[b]*College of Chemistry and Environmental Science, Lanzhou City University, Lanzhou 730070, China.*

E-mail: magf@nwnu.edu.cn (G. Ma); Leizq@nwnu.edu.cn (Z. Lei)

Abstract

Cotton-based porous activated carbons (CACs) are prepared through a simple chemical activation method using cotton fiber as carbon source and $ZnCl_2$ as activating agent. The powder X-ray diffraction, scanning electron microscopy, and N_2 adsorption-desorption test demonstrate that the carbons activated with different amounts of $ZnCl_2$ have large number of mesopores, notably, a maximum specific surface area of 2548.6 m^2 g^{-1} and ultrahigh pore volume of 1.54 cm^3 g^{-1} for CAC2 sample is obtained when the cotton/$ZnCl_2$ mass ratio is 1:2. As an electrode material for supercapacitors, the CAC2 possesses high specific capacitance of 239 F g^{-1} at 0.5 A g^{-1} and good rate capability (82% capacitance retention even at 8 A g^{-1}) in 2 mol L^{-1} KOH aqueous electrolyte. Moreover, the as-assembled CAC2//CAC2 symmetric supercapacitor exhibits high energy density of 13.75 Wh kg^{-1} at a power density of 225 W kg^{-1} operated at the voltage range of 0 to 1.8 V in 0.5 mol L^{-1} Na_2SO_4 aqueous electrolyte and an excellent cyclability retaining about 93% initial capacitance after 5000 cycles.

Keywords: Cotton, Activated carbon, Chemical activation, Supercapacitor

1. Introduction

Supercapacitors, a new class of electrical energy storage devices with high power density, long cycle life, rapid charge/discharge rates and high safety etc., have attracted intense attention over the past decades owing to their widespread applications, such as hybrid electric vehicles, portable electronic equipment and uninterruptible power supplies [1-3]. The performances of supercapacitors are largely dependent on the properties and structures of the electrode materials. Basing on mechanism of charge storage, supercapacitors can be categorized in two major classes, i.e., electrochemical double-layer capacitor (EDLC) and pseudocapacitor. The capacitance of EDLC comes from non-faradic charge accumulation at interfacial double layer of electrode and electrolyte, whereas in pseudocapacitors, reversible faradic redox reactions also add up the capacitance along with non-faradic charge [4-7]. Transition metal oxides or hydroxides, such as RuO_2, MnO_2, $Ni(OH)_2$, etc., and conductive polymers have been used to increase the specific capacitance via a variety of reversible oxidation states for highly efficient redox charge transfer [8-10]. However, low electrical conductivity, poor cycle stability and high price have limited the practical application of those pseudocapacitive materials [11-13]. Carbon materials with porous structure, large surface area, high conductivity, and long-term cycle ability, etc., having always been regarded as the most promising candidate electrode materials for electrical energy storage devices [14-18].

To date, carbon materials in nature have been investigated extensively as potential electrode materials for supercapacitors. Bamboo [19], coconut shell [20], peanut shell [21], celtuce [22] and lignin [23] have been considered as possible precursors for the synthesis of activated carbons.

Cotton is known as one of the most important agricultural commodities, which is widely cultivated and abundant production. Wang et al. have prepared cotton-based hollow carbon fibers (CCFs) by ammonia etching for supercapacitor application. The CCFs obtained by carbonization in NH_3 has high specific surface area up to 778.6 m^2 g^{-1}, higher nitrogen concentration (3.3 at%) and more C=O functional groups, but ammonia is corrosive in the preparation process. Therefore, it is significant to find an eco-friendly method to make carbon materials. Herein, we prepared cotton-based porous activated carbons (CACs) through a simple chemical activation method using cotton fiber as carbon source and $ZnCl_2$ as activating agent, and a maximum specific surface area up to 2548.6 m^2 g^{-1} for CAC2 sample was obtained when the cotton/$ZnCl_2$ mass ratio is 1:2, which is higher than that of 778.6 m^2 g^{-1} for CCFs. Additionally, in our work, the mass ratio between the cotton and activating agent which can affect the carbons structure and morphology was studied, and the performance of the supercapacitor using CAC2 as electrode was also investigated.

2. Experimental

2.1. Synthesis of CACs samples

Materials: Medical absorbent cotton (MAC, Zhongtai Medical Device Co., Ltd., Hebei, China), zinc chloride ($ZnCl_2$, Aladdin Ltd., Shanghai, China). All chemical reagents were in analytical grade.

In a typical synthesis, 1.0 g of the medical absorbent cotton (MAC) was mixed with $ZnCl_2$ in different proportions (MAC/$ZnCl_2$ mass ratio is 1:0, 1:1, 1:2, 1:3, respectively) in 50 mL of distilled water and dipped at 80 °C under magnetic stirring for 5 h, and the mixtures were dried at 80 °C, then, carbonized the mixtures at optimum temperature 900 °C for 2 h with temperature ramp rate of 5 °C min^{-1} under high pure N_2 atmosphere. After being cooled to room temperature

naturally, the carbide samples were thoroughly washed with 2 mol L^{-1} HCl to remove inorganic salts and other impurities. Finally, the samples were washed with distilled water until neutral pH and dried at 60 °C for 24 h. The obtained samples of different activation proportions with $ZnCl_2$ were designated as CAC0, CAC1, CAC2 and CAC3, respectively.

In order to optimize the best carbonization temperature, we adopt 1.0 g MAC without $ZnCl_2$ for preparation of cotton-based carbon material at the different carbonization temperatures (700, 800, 900 or 1000 °C). The other preparation process is the same as the CACs. The samples were marked as CAC-x, where x is the carbonization temperature.

2.2. Materials Characterization

A field emission scanning microscope (FE-SEM, Ultra Plus, Carl Zeiss, Germany) was used to examine the morphologies and structures of the carbon samples. The Brunauer-Emmett-Teller (BET) surface area (S_{BET}) of the samples were analyzed by nitrogen adsorption in a Micromeritics ASAP 2020 nitrogen adsorption apparatus (U.S.A.). X-ray diffraction (XRD) of sample was performed by a diffractometer (D/Max-2400, Rigaku) and Raman spectra was recorded with an in Via Raman spectrometer (Renishaw).

2.3. Electrochemical measurement

2.3.1. Three-Electrode Cell Fabrication

In a three-electrode system, a 5 mm diameter glassy carbon electrode was adopted as the working electrode, Hg/HgO electrode serves as the reference electrode and carbon rod as the counter electrode, respectively. The working electrodes were prepared similarly to our former reported literature [24]. Typically, 4.0 mg of activated materials (CACs) were dispersed ultrasonically in 0.4 mL of 0.25 wt% Nafion (DuPont, Wilimington, DE, U.S.A.) ethanol solution,

using a pipet gun to suck up the above uniform suspension of 8.0 μL and drop onto the surface of a glassy carbon electrode, and dried at room temperature. Then, the three-electrode system was tested in 2 mol L^{-1} KOH aqueous electrolyte.

2.3.2. Two-Electrode Cell Fabrication

For a two-electrode system, the working electrode was prepared by mixing the CAC2 with binder polyvinylidene fluoride (PVDF) and commercial carbon black in a mass ratio of 8:1:1 and homogenizing slurry in N-methyl-2-pyrrolidone (NMP) solution. Further, the obtained slurry was coated on the nickel foam with an area of 1.0 cm^2 and dried at 60 °C for 24 h, and then weighted and pressed into sheets under 15 MPa. The total mass of each electrode was limited to vary from 3.0 to 5.0 mg and we chose the two electrodes with identical or very close weight for the measurements [25]. The CAC2 electrode fitted with the separator (thin polypropylene film) and electrolyte solution were symmetrically assembled into sandwich-type cells construction (electrode/separator/electrode). In order to make aqueous electrolyte solutions homogeneously diffuse into the CAC2 electrodes, the separator and CAC2 electrodes were immersed in 0.5 mol L^{-1} Na_2SO_4 electrolyte for 12 h before being assembled into the supercapacitor configuration.

The electrochemical properties of electrodes were analyzed by cyclic voltammetry (CV), galvanostatic charge/discharge and electrochemical impedance spectroscopy (EIS) measurements in three-electrode cell and two-electrode configuration using an electrochemical workstation system (CHI 660D, Shanghai Chen Hua Co. Ltd., China). The cycle-life stability was recorded using cycling testing equipment (CT2001A, Wuhan Land Electronic Co. Ltd., China).

3. Results and discussions

The as-prepared cotton-based activated carbons (CACs) as electrode materials for supercapacitors application, and carbonization temperature seriously affect their electrochemical characters. Thus, the cyclic voltammograms (CVs) of carbon electrodes from different carbonization temperatures were measured at a scan rate of 50 mV s^{-1} with the potential range of -1.0 to 0 V in 2 mol L^{-1} KOH aqueous electrolyte (**Figure 1**). It can be seen that the CV curves of CACs gradually approach rectangular shape with the increase of carbonization temperature. Obviously, the carbon samples carbonized with low temperature (700 ^{o}C and 800 ^{o}C) exhibit small irregular rectangular curves corresponding to low current response behavior due to their poor electrical conductivity. In contrast, the CV curves of CACs treated with high temperature (900 ^{o}C and 1000 ^{o}C) exhibit quasi-rectangular shape, indicating ideal capacitive behavior. But, as the carbonization temperature is increased up to 1000 °C, the curve area is obviously reduced, which may be caused by the collapse and stack of some carbon skeletons. Therefore, 900 ^{o}C is the best carbonization temperature of cotton fiber, and the MAC mixed with $ZnCl_2$ in different proportions were all carbonized at 900 ^{o}C and used for supercapacitor applications unless otherwise specified.

3.1. The morphologies and structures of CACs samples

Figure 2a-d show the typical SEM images of CACs samples, and different surface morphologies are observed for all carbon samples. The CAC0 presents a shape of highly distorted bar structure, and has slightly wrinkled surface without apparent pores (**Figure 2a**). However, when treated with $ZnCl_2$, the surface morphologies of carbon samples are changed. The CAC1 presents uneven and rough surface (**Figure 2b**). More interestingly, the CAC2 displays rich loose and porous morphology (**Figure 2c**). Furthermore, after treated with excessive $ZnCl_2$, the CAC3 exhibits abundant macroporous structure (**Figure 2d**). These results indicate that the $ZnCl_2$

activation agent can play an important role in forming porous structure during the carbonization process.

The nitrogen adsorption-desorption isotherms and pore size distribution curves of CACs are shown in **Figure 3a-b**. As presented in **Figure 3a**, the nitrogen adsorption-desorption isotherms of all CACs are presented type IV with a H3 hysteresis loop in the range of ca. 0.40-0.99 P/P_0, which suggests the CACs have mesoporous structures. Moreover, there are also clearly defined step loops in the relative pressure region between 0.4 and 0.6, demonstrating the CACs possess uniform mesoporous structures [26]. Meanwhile, at low relative pressure ($P/P_0 < 0.40$), the adsorption isotherms of CACs are rapidly saturated, suggesting the adsorption of micropores. In addition, we can find out that as the mass ratio of MAC/$ZnCl_2$ increased from 1:0 to 1:2, the adsorbed volume of CACs increase clearly. Comparing CAC0 and CAC1 samples, the CAC2 has higher adsorbed volume. However, it is found that the adsorbed volume of CAC3 significant decreases due to the large cavities presence caused by excessive $ZnCl_2$. The specific surface area, pore volume, and average pore size of CACs obtained by BET measurement are summarized in **Table 1**. Particularly, the specific surface area and total pore volume of CAC2 are 2548.6 $m^2 g^{-1}$ and 1.54 $cm^3 g^{-1}$, respectively. The pore size distribution curves (**Figure 3b**) imply that the CAC2 has abundant mesoporous pores. The large specific surface areas and high pore volumes of CAC2 are beneficial to ion transfer and charge storage for supercapacitors.

Figure 3c is the XRD pattern of CAC2. Two broad diffraction peaks at 22.1° and 43.1° are observed, ascribing to the (002) and (100) crystal planes of graphitic carbon, which suggests the low graphitization degree and the possible presence of amorphous carbon [27]. The Raman spectrum of CAC2 is shown in **Figure 3d**. It shows two distinct peaks at 1344 (D-band) and 1603

cm^{-1} (G-band). These bands correspond to the disordered carbon/structural defects and graphitic layers (sp^2 bonded carbon atoms) of the carbon material [28]. Increased G-band intensity compared to D-band ($I_D/I_G = 0.96$) confirms that the formation of long-range graphitized carbon with a relatively small number of structural defects.

3.2. Electrochemical characteristics of CACs electrodes

A three-electrode system was used to evaluate the electrochemical properties of the CACs. **Figure 4a** is the CV curves of CACs electrodes at a scan rate of 50 mV s^{-1} with the potential range of -1.0 to 0 V. Clearly, the CAC2 exhibits larger area than that of others indicating CAC2 has the greatest specific capacitance, according to the linear relationship between CV curve area and specific capacitance. In addition, the CV curves of CAC2 retain quasi-rectangular shape even at a scan rate of up to 100 mV s^{-1} (**Figure 4b**), suggesting the CAC2 exhibits a high rate capability.

To calculate the specific capacitance of the CAC2 electrode, the galvanostatic charge/discharge measurement was carried out, and the result is shown in **Figure 4c**. All the curves are highly symmetrical at different current densities, suggesting that the CAC2 possesses excellent electrochemical reversibility and charge/discharge properties. The specific capacitance of electrodes can be calculated using the following equation [29]:

$$C_m = (It)/(\Delta V m) \quad (1)$$

where C_m is specific capacitance (F g^{-1}), I is charge/discharge current (A), t is the time of discharge (s), ΔV is the voltage difference between the upper and lower potential limits, and m is the mass of the active electrode material. According to the above calculating formula of specific capacitance, the correlation between the specific capacitance and the various current densities for different electrodes is shown in **Figure 4d**. It exhibits that the highest specific capacitance of

CAC2 is 239 F g^{-1} at 0.5 A g^{-1}, and 196 F g^{-1} even at 8 A g^{-1}, which remains about 82% of the highest capacitance. The result indicates that the high capacitance of CAC2 electrode can be maintained under higher current density.

Electrochemical impedance spectroscopy (EIS) measurements of the CACs electrodes are shown in **Figure 5a**. Contrasting the Nyquist plots, the CAC2 electrode presents smaller semicircle at the high frequency region and more vertical line at the low frequency region, which means that the CAC2 has low ion-transport resistance and ideal capacitor behavior than other electrodes.

The two-electrode symmetric supercapacitor was also fabricated to further assess the actual electrochemical performance of CAC2 electrode. Compared with the acid and alkali solutions, the neutral Na_2SO_4 aqueous electrolyte has a higher operation voltage [30]. CV cures of the CAC2//CAC2 symmetric cell in comparison to Ni foam at the same potential window is shown in **Figure 5b**. It can be seen that the CV curve of Ni foam nearly approaches linear shape, indicating that Ni foam has no effect on the electrochemical properties of CAC2. Therefore, the working electrode CAC2 was prepared by coating on the Ni foam in the two-electrode system, and the CAC2//CAC2 symmetric supercapacitor was assembled and characterized in 0.5 mol L^{-1} Na_2SO_4 aqueous electrolyte. **Figure 6a** shows the CV curves of the symmetric cell at different voltage windows. When the high voltage extends to 1.8 V, the CV curves of the supercapacitor still retain rectangular-like shape indicating ideal capacitive behavior and good reversibility. However, when the voltage increases to 2.0 V, the current is dramatically increased since the electrolyte is being decomposed with hydrogen and/or oxygen evolution [31]. Therefore, the potential window of 1.8 V is selected to measure the electrochemical performance of the symmetric cell. The CV curves of

the symmetric cell obtained at different scan rates from 10 to 100 mV s^{-1} at the voltage range of 0 to 1.8 V are shown in **Figure 6b**, we can see that the CV curve area still keep a quasi-rectangular shape even at a scan rate of 100 mV s^{-1}. **Figure 6c** displays galvanostatic charge/discharge curves of the symmetric cell at different current densities from 0.25 to 8 A g^{-1}. Using the following formulas [25], the specific energy density (E, Wh kg^{-1}) and power density (P, W kg^{-1}) for a supercapacitor cell were counted.

$$E = {}^{1}/_{2}CV^{2} \quad (2)$$

$$P = E/t \quad (3)$$

where C is the specific capacitance of the cell (F g^{-1}), V is the voltage change during the discharge process after the IR drop in galvanostatic discharge curve, t is the time of discharge (s). For comparison, we used ordinary activated carbon (AC) to fabricate AC//AC symmetric cell and evaluate its electrochemical performance under the same conditions. The result shows that the CAC2//CAC2 symmetric cell exhibits the highest energy density of 13.75 Wh kg^{-1} with a power density of 225 W kg^{-1}, which higher than the highest energy density of 7.31 Wh kg^{-1} with a power density of 225 W kg^{-1} of the AC//AC symmetric cell. Ragone plots of the CAC2//CAC2 symmetric cell in comparison to AC//AC symmetric cell are shown in **Figure 6d**. Moreover, the obtained maximum energy density of 13.75 Wh kg^{-1} is also higher than those of recently reported symmetric cells, such as AC//AC (10 Wh kg^{-1}) [32], MC//MC (7.84 Wh kg^{-1}) [33], and MCSF//MCSF (9.6 Wh kg^{-1}) [34].

As shown in **Figure 7a**, the Nyquist plot of the CAC2//CAC2 symmetric cell indicates that the CAC2 possesses high electrical conductivity with a small ESR of 1.50 Ω. The stability and reversibility of electrode material are important for its use in electrochemical supercapacitors.

Figure 7b displays the capacitance retentions versus cycle number curves of the CAC2//CAC2 symmetric cell at a current density of 5 A g^{-1}. As can be observed, the symmetric cell displays satisfactory cycling stability with about 93% specific capacitance remaining after 5000 cycles.

4. Conclusions

In summary, porous activated carbons from cotton fiber (CACs) have been successfully prepared in a simple chemical activation method. By optimizing the carbonization temperature and the amount of $ZnCl_2$ activating agent, the resulting porous carbon (CAC2) shows an extremely high specific surface area of up to 2548.6 m^2 g^{-1} as well as high capacitive performance with a specific capacitance of 239 F g^{-1} in three-electrode systems. Furthermore, the as-assembled CAC2//CAC2 symmetric supercapacitor device with an wide operation voltage of 0 to 1.8 V in 0.5 mol L^{-1} Na_2SO_4 aqueous electrolyte delivers a high energy density of 13.75 Wh kg^{-1}, and excellent cycling performance (only 7% capacitance loss after 5000 cycles). Therefore, it is a promising strategy to synthesize CACs electrode materials with low cost and eco-friendly for high-performance supercapacitor applications.

Acknowledgements

The research was financially supported by the Science and Technology program of Gansu Province (NO.1308RJZA295, 1308RJZA265, 1308RJZA103), the National Science Foundation of China (NO.21164009, 21174114), the program for Changjiang Scholars and Innovative Research Team in University (IRT1177).

References

[1] M. F. El-Kady, V. Strong, S. Dubin and R. B. Kaner, *Science*, 2012, 335, 1326-1330.

[2] B. Dyatkin, V. Presser, M. Heon, M. R. Lukatskaya, M. Beidaghi and Y. Gogotsi, *ChemSusChem*, 2013, 6, 1169-2280.

[3] G. P. Wang, L. Zhang and J. J. Zhang, *Chem. Soc. Rev.*, 2012, 41, 797-828.

[4] H. L. Wang, H. S. Casalongue, Y. Y. Liang and H. J. Dai, *J. Am. Chem. Soc.*, 132, 2010, 7472-7477.

[5] D. Bhattacharjya and J. S. Yu, *J. Power Sources*, 2014, 262, 224-231.

[6] V. Augustyn, P. Simon and B. Dunn, *Energy Environ. Sci.*, 2014, 7, 1597-1614.

[7] H. Jiang, P. S. Lee and C. Z. Li, *Energy Environ. Sci.*, 2013, 6, 41-53.

[8] X. H. Lu, M. H. Yu, G. M. Wang, T. Zhai, S. L. Xie, Y. C. Ling, Y. X. Tong and Y. Li, *Adv. Mater.*, 2013, 25, 267-272.

[9] Y. G. Li, H. L. Wang, L. M. Xie, Y. Y. Liang, G. S. Hong and H. J. Dai, *J. Am. Chem. Soc.*, 2011, 133, 7296-7299.

[10] Z. Li, Z. W. Xu, H. L. Wang, J. Ding, B. M. Zahiri, C. M. B. Holt, X. H. Tan and D. Mitlin, *Energy Environ. Sci.*, 2014, 7, 1708-1718.

[11] G. A. Snook, P. Kao and A. S. Best, *J. Power Sources*, 2011, 196, 1-12.

[12] W. J. Qian, F. X. Sun, Y. H. Xu, L. H. Qiu, C. H. Liu, S. D. Wang and F. Yan, *Energy Environ. Sci.*, 2014, 7, 379-386.

[13] J. Jiang, Y. Y. Li, J. P. Liu, X. T. Huang, C. Z. Yuan and X. W. D. Lou, *Adv. Mater.*, 2012, 24, 5166-5180.

[14] J. P. Paraknowitsch and A. Thomas, *Energy Environ. Sci.*, 2013, 6, 2839-2855.

[15] J. P. Liu, J. Jiang, C. W. Cheng, H. X. Li, J. X. Zhang, H. Gong and H. J. Fan, *Adv. Mater.*, 2011, 23, 2076-2081.

[16] G. X. Luo, L. Z. Liu, J. F. Zhang, G. B. Li, B. L. Wang and J. J. Zhao, *ACS Appl. Mater. Inter.*, 2013, 5, 11184-11193.

[17] V. K. Gupta, I. Ali, T. A. Saleh, M. N. Siddiqui and S. Agarwal, *Environ. Sci. Pollut. R.*, 2013, 20, 1261-1268.

[18] Z. Li, L. Zhang, B. S. Amirkhiz, X. H. Tan, Z. W. Xu, H. L. Wang, B. C. Olsen, C. M. B. Holt and D. Mitlin, *Adv. Energy Mater.*, 2012, 2, 431-437.

[19] C. S. Yang, Y. S. Jang and H. K. Jeong, *Curr. Appl. Phys.*, 2014, 14, 1616-1620.

[20] K. Jurewicz and K. Babe, *Energ. Fuel.*, 2010, 24, 3429-3435.

[21] M. B. Wu, R. C. Li, X. J. He, H. B. Zhang, W. B. Sui and M. H. Tan, *Carbon*, 2015, 86, 371-374.

[22] R. T. Wang, P. Y. Wang, X. B. Yan, J. W. Lang, C. Peng and Q. J. Xue, *ACS Appl. Mater. Inter.*, 2012, 4, 5800-5806.

[23] D. Saha, Y. C. Li, Z. H. Bi, J. H. Chen, J. K. Keum, K. Dale, S. Dai and A. K. Naskar, *Langmuir*, 2014, 30, 900-910.

[24] H. Peng, G. F. Ma, K. J. Sun, J. J. Mu and Z. Q. Lei, *J. Phys. Chem. C*, 2014, 118, 29507-29516.

[25] H. Peng, G. F. Ma, K. J. Sun, J. J. Mu and Z. Q. Lei, *ACS Appl. Mater. Inter.*, 2014, 6, 20795-20803.

[26] B. Xu, H. Duan, M. Chu, G. P. Cao and Y. S.Yang, *J. Mater. Chem. A*, 2013, 14, 4565-4570.

[27] P. P. Su, L. Jiang, J. Zhao, J. W. Yan, C. Li and Q. H. Yang, *Chem. Commun.*, 2012, 48, 8769-8771.

[28] M. G. Hahm, A. M. R. Leela, D. P. Cole, J. A. Vento, M. Rivera, J. Nam and R. Vajtai, *Nano Lett.*, 2012, 12, 5616-5621.

[29] G. F. Ma, H. Peng, J. J. Mu, H. H. Huang, X. Z. Zhou and Z. Q. Lei, *J. Power Sources*, 2013, 229, 72-78.

[30] Q. Wang, J. Yan, Y. B. Wang, T. Wei, M. L. Zhang, X. Y. Jing and Z. J. Fan, *Carbon*, 2014, 67, 119-127.

[31] Y. P. Zhai, Y. Q. Dou, D. Y. Zhao, P. F. Fulvio, R. T. Mayes and S. Dai, *Adv. Mater.*, 2011, 23, 4828-4850.

[32] L. Demarconnay, E. Raymundo-Pinero and F. Béguin, *Electrochem. Commun.*, 2010, 12, 1275-1278.

[33] X. J. He, R. C. Li, J. S. Qiu, K. Xie, P. H. Ling, M. X. Yu, X. Y. Zhang and M. D. Zheng, *Carbon*, 2012, 50, 4911-4921.

[34] Q. Wang, J. Yan, T. Wei, J. Feng, Y. M. Ren, Z. J. Fan, M. L. Zhang and X. Y. Jing, *Carbon*, 2013, 60, 481-487.

Figure captions:

Figure 1. CV curves of cotton carbon materials synthesized at different carbonization temperatures at a scan rate of 50 mV s^{-1}.

Figure 2. SEM images of the carbon samples treated with $ZnCl_2$ activating agent in different proportions: (a) CAC0, (b) CAC1, (c) CAC2 and (d) CAC3, respectively.

Figure 3. (a) Nitrogen adsorption-desorption isotherms and (b) Pore size distribution curves of CACs, (c) X-ray diffraction pattern and (d) Raman spectrum of the CAC2.

Figure 4. (a) CV curves of CACs electrodes at a scan rate of 50 mV s^{-1}, (b) CV curves of the CAC2 electrode at various scan rates, (c) Galvanostatic charge/discharge curves of the CAC2 electrode at various current densities, (d) Specific capacitance as a function of the current densities of the CAC2 electrode.

Figure 5. (a) Nyquist plots of the CACs electrodes and their expanded high frequency region (inset), (b) CV curves of the CAC2//CAC2 symmetric cell in comparison to Ni foam//Ni foam symmetric cell at 50 mV s^{-1} with the potential range of 0 to 1.8 V.

Figure 6. (a) CV curves of the CAC2 symmetric cell at different voltage windows at a scan rate of 50 mV s^{-1}, (b) CV curves of the CAC2 symmetric cell at various scan rates with the potential range of 0 to 1.8 V, (c) Galvanostatic charge/discharge curves of the CAC2 symmetric cell at various current densities, (d) Ragone plot of the CAC2//CAC2 symmetric cell in comparison to AC//AC symmetric cell.

Figure 7. (a) Nyquist plots of CAC2 symmetric cell, (b) Cycling stability of CAC2 symmetric cell at 5 A g^{-1}.

Table 1 The BET measurement summary of cotton carbon samples (CACs).

Figure 1

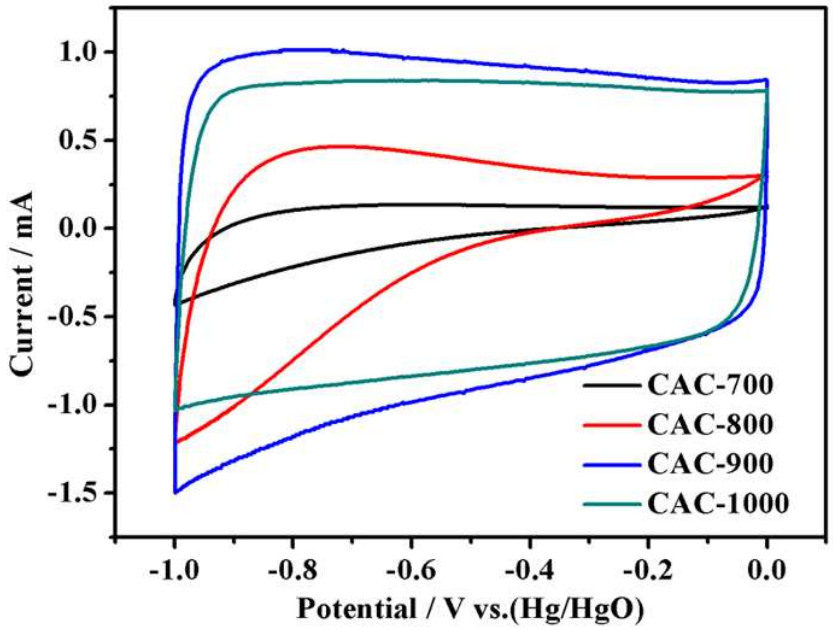

Figure 2

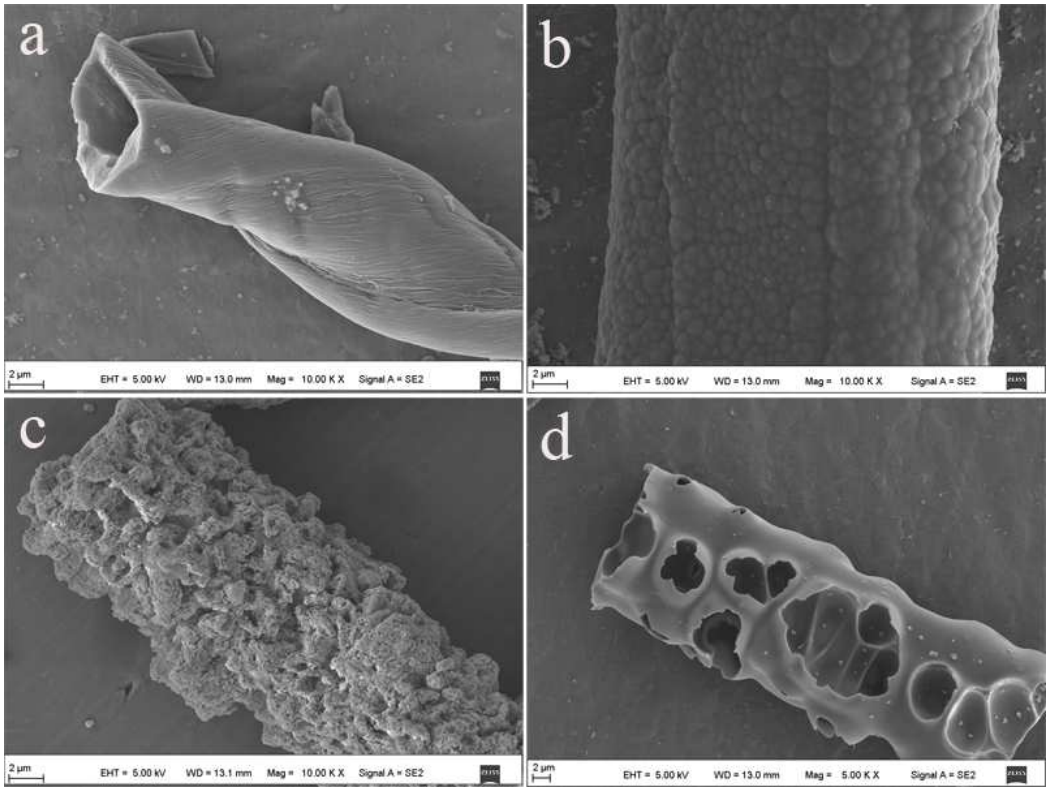

Figure 3

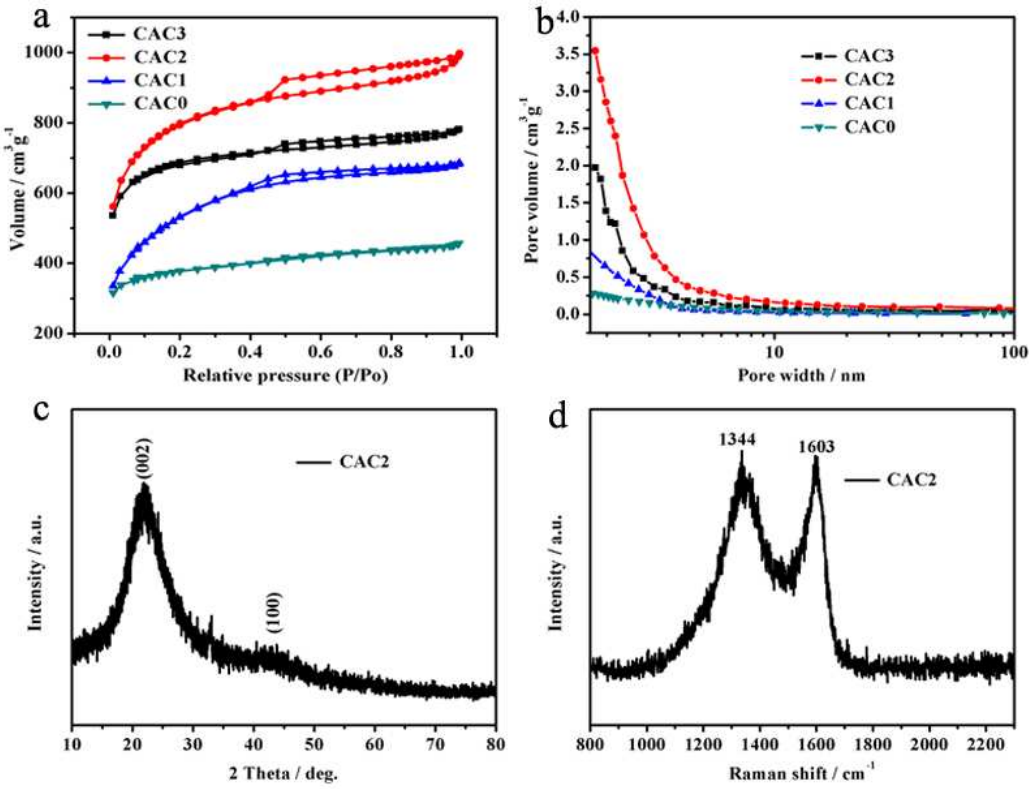

Figure 4

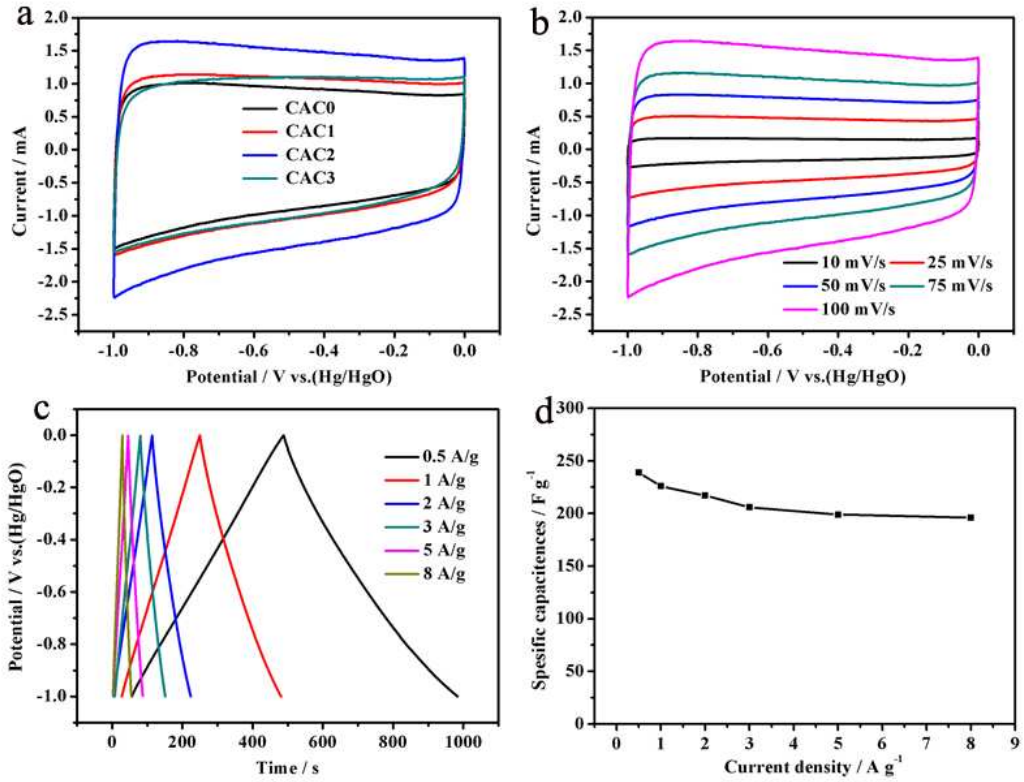

Figure 5

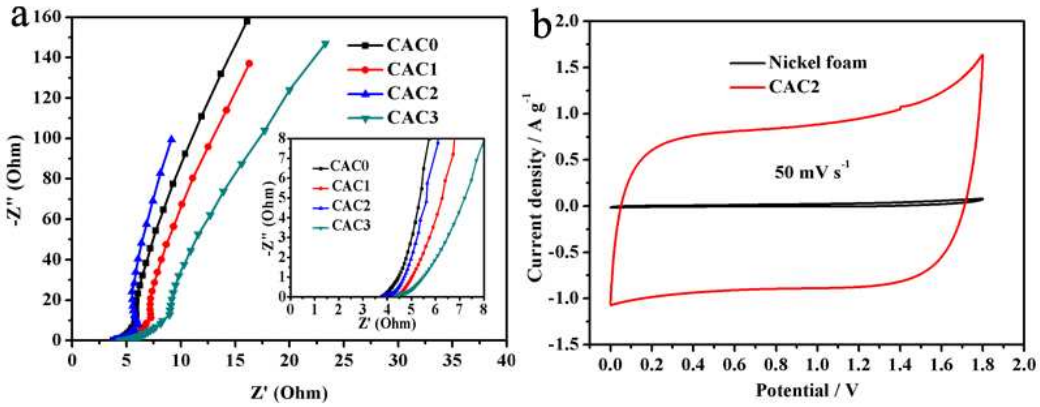

Figure 6

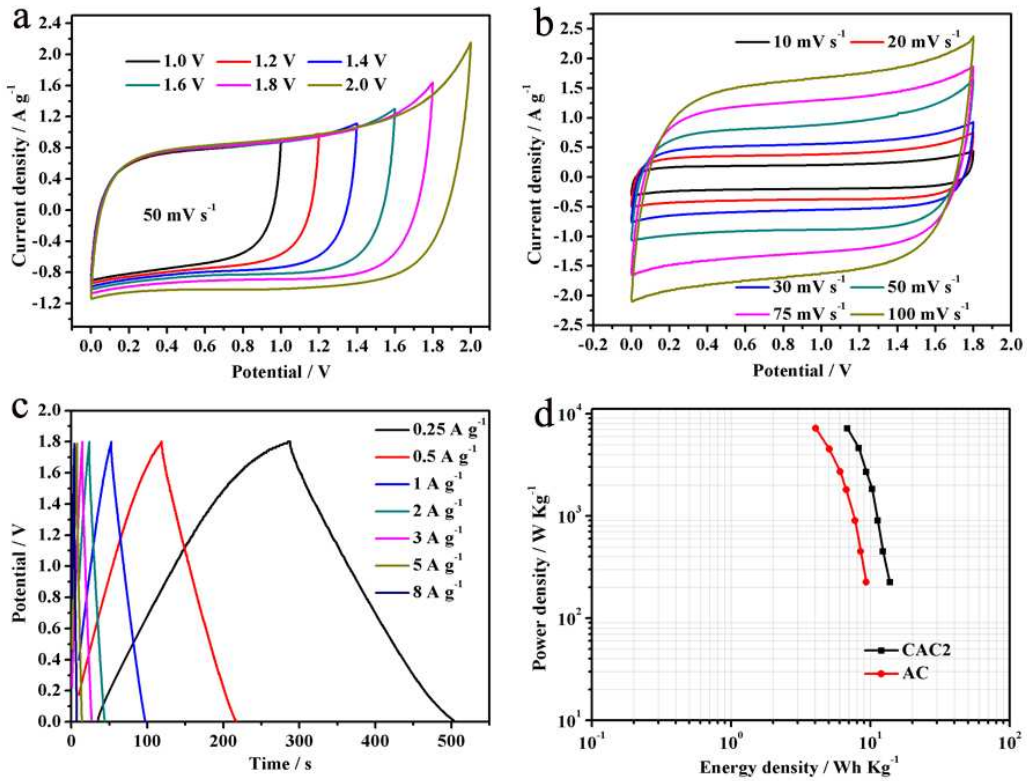

Figure 7

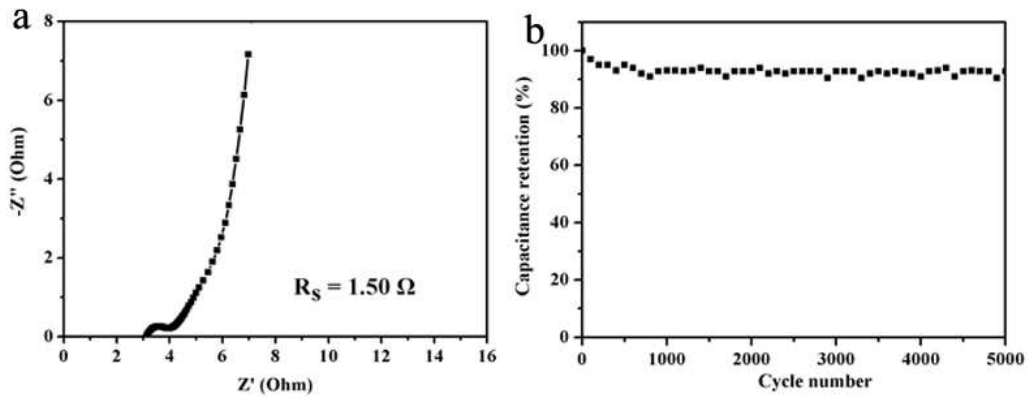

Table 1

Samples	S_{BET}[a] (m^2 g^{-1})	Pore volume[b] (cm^3 g^{-1})	Average pore size (nm)
CAC0	1169.5	0.71	2.41
CAC1	2121.9	1.21	2.28
CAC2	2548.6	1.54	2.42
CAC3	1793.5	1.06	2.36

[a] Specific surface area from multiple BET method.

[b] Total pore volume at $P/P_0 = 0.99$.

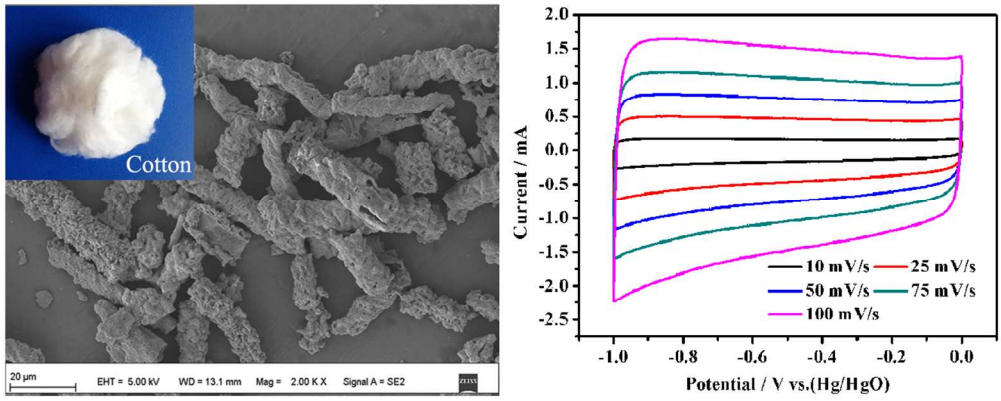

351x140mm (96 x 96 DPI)